Surface Potential and Morphology Mapping to Investigate Analyte Adsorption Effects on Surface Enhanced Raman Scattering (SERS)

Abhijit Chatterjee, David J G Gale, Dmytro Grebennikov, Liam D Whelan and Erika F Merschrod S*

1 ZnO film synthesis

100 mL of 0.05 M zinc acetate, dihydride ($ZnOAc_2 \cdot 2\,H_2O$ $\geq$99.0%, J T Baker Inc.) solution and 100 mL of 1.5 M NaOH (99%, Sigma Aldrich) solution were prepared in ultrapure water (Barnstead, 18.2 MΩ·cm). The NaOH solution was then added to the zinc acetate solution, which generated zinc hydroxide. Afterwards, acid cleaned glass slides cut to 2×2 cm^2 were placed horizontally at the bottom of the solution beaker. The solution was then heated for 30 minutes at 35°C, which resulted in a white turbid appearance. After the heating process, the solution was kept at room temperature for 6 hours, while generating a ZnO thin film on the glass slides. The coated slides were washed with ultrapure water and air dried. A quartz crystal microbalance (INFICON XTM/2 deposition monitor) was used to monitor metal thickness during gold vapor deposition (locally-built instrument).

2 XRD and SEM instrumental details

X-ray diffraction (XRD) characterization of samples was conducted using the Rigaku Ultima-IV instrument with a Cu K-α source at 40 kV and 44 mA.

Field emission scanning electron microscopy (FESEM) images were acquired using a JEOL JSM-7100F equipped with a field emission source at 15 kV potential.

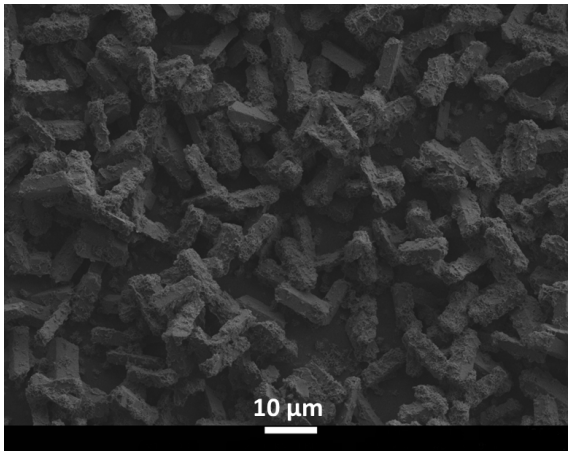

Figure S1: SEM image of a film of rod shaped ZnO crystals, taken at lower magnification than the image in Figure 1 in the main paper.

3 Raman analysis

All Raman spectra were collected with a Renishaw In-via Raman microscope using 20× magnification and a 40 s exposure time of the 830 nm laser source at 3.0 ± 0.3 mW power. Figure S2 shows a Raman spectrum of a ZnO sample.

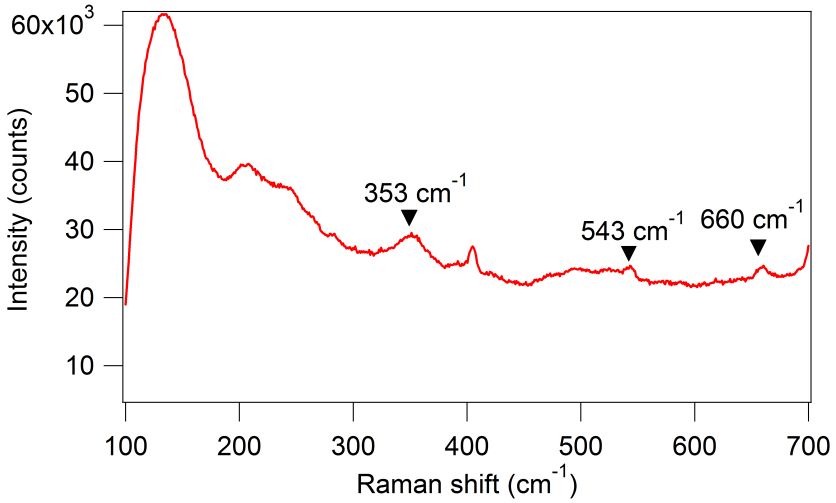

Figure S2: Raman spectrum of ZnO shows three characteristic ZnO Raman peaks.

The Raman spectrum (Figure S2) of as-prepared ZnO shows a shift in the A_1(LO) mode. A shift like this could arise from atom vacancies, strain due to crystal lattice mismatch, or the presence of dopants or contaminants. In this case, a red shifted A_1(LO) mode arises from intrinsic defects.[1] The other Raman peaks at 353 cm^{-1}, 543 cm^{-1} and 660 cm^{-1} correspond to (E_2-E_1), E_1(LO)/A_1(LO) and Zn sublattice vibration modes, respectively.[2]

4 Plasmon absorption of different substrates

Plasmon optical absorption was conducted with an Ocean Optics USB 2000 spectrophotometer using diffuse reflectance. Absorption intensity was calculated from the percent reflectance (%R) using the Kubelka-Munk equation.[3]

$$\frac{K}{S} = \frac{(1-R)^2}{2R} \tag{S1}$$

where K is the absorption coefficient and S is the scattering coefficient.

The plasmon appears in the UV-visible absorption spectrum as a broad peak. Comparable excitation wavelength and plasmon absorption wavelength could contribute to signal enhancement,[4] and we do see plasmon absorption in the near-IR region in Figure S3. Nevertheless, although the plasmon absorption intensity changes with thickness, the changes are not enough to explain the difference in SERS activity.

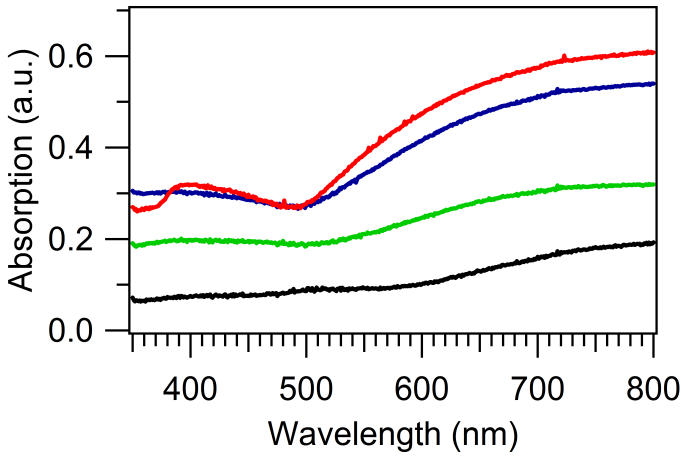

Figure S3: Optical absorption of different thicknesses of Au covered ZnO shows higher plasmon absorption of A45 (red) and A35 (blue) over A15 (green) and A25 (black).

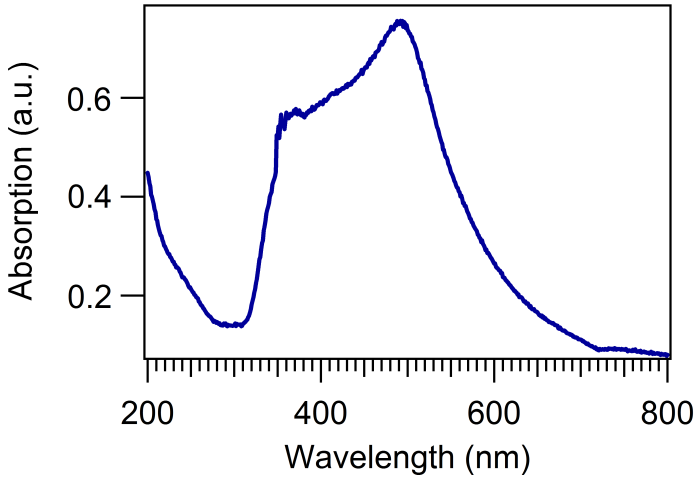

Figure S4: The plasmon absorption spectrum of a 35 nm thick Au film on glass alone does not show any absorption near the Raman excitation wavelength. This spectrum was recorded using a transmission geometry since Au on glass generates a relatively transparent film.

5 Enhancement factor (EF) calculations

For the enhancement factor calculation,[5] the reference substrate for the normal Raman measurement was a glass slide exposed to a 0.1 M aqueous phenanthrene solution for thirty minutes. Because of the weak adsorption of phenanthrene to glass, the analyte was no longer detectable after rinsing even at such high concentrations. Therefore, the reference samples were not rinsed before drying, and we may be *under*estimating our enhancement factors.

The enhancement factor calculation used the vibrational mode at 705 cm^{-1} due to its high intensity.

$$\mathrm{EF} = \frac{\mathrm{I}_{SERS}}{\mathrm{C}_{SERS}} \times \frac{\mathrm{C}_{Normal}}{\mathrm{I}_{Normal}} \tag{S2}$$

I_{SERS} and I_{Normal} are the intensities of the surface enhanced Raman mode and the normal Raman mode, respectively. C_{SERS} and C_{Normal} are the concentrations of the analyte in the SERS and the normal Raman measurements, respectively.

The Raman spectra for phenanthrene adsorbed from various concentration solutions are shown in Figure S5, using the A35 substrate. Raman signal intensity (peak height relative to baseline) decreases when lowering the phenanthrene concentration. Nevertheless, the peak is still detectable even at a concentration of 0.001 ppm (or 1 ppb).

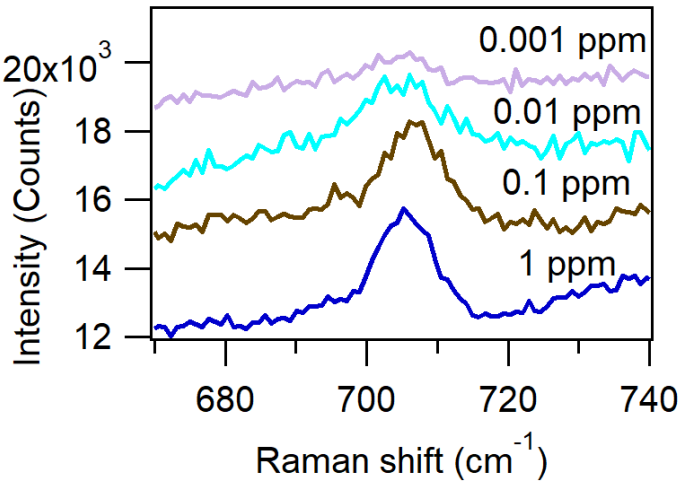

Figure S5: A comparison of Raman signal at 705 cm^{-1} for phenanthrene solutions of 1 ppm, 0.1 ppm, 0.01 ppm and 0.001 ppm (1 ppb). The spectra are offset for clarity.

6 SERS activity of only Au and only ZnO

The Raman spectra from control experiments with a 35 nm thick Au film or ZnO film (on glass) show no SERS activity (no analyte peaks after exposure to 1 ppm of phenanthrene). The spectra are shown in Figure S6.

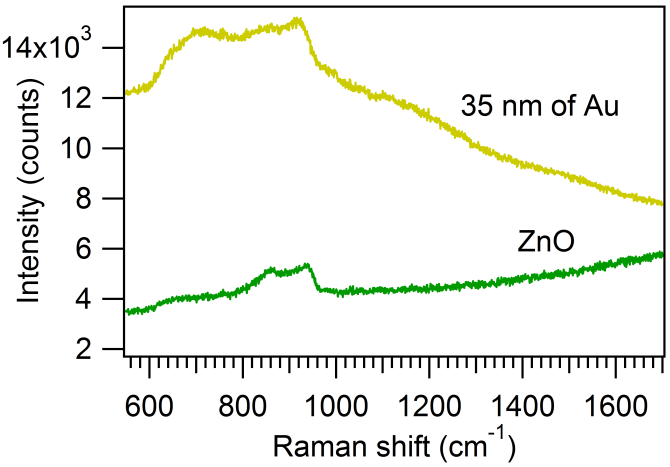

Figure S6: Both Au and ZnO films alone are SERS inactive.

7 Surface area, roughness, and work function measurements

A Pt coated tip (Mikromasch NSC35/Pt; resonance frequency = 300 KHz and force constant = 16 N/m) was used for KPFM with the MFP-3D (Asylum Research) instrument. All scans were performed with 256 points per line and 256 lines per image at a 0.5 Hz scan rate.

The samples involve Au deposited on top of a ZnO nanorod film; the Au layer is not conformal. Therefore, during the scan the tip interacts with gold, but it also encounters bare ZnO at crystal edges. This is consistent with the significant difference between the work functions near the center and at the edges of the crystals (Figure 4 in main article). Six different 1 μm^2 areas were selected on top of a Au covered nanorod to calculate the work function as well as the surface area (Figure S7). By avoiding the very edges but considering several regions, we ensure that we are truly measuring the work function of Au on ZnO in each case, while still capturing the possible variation in work function across a Au-covered ZnO rod.

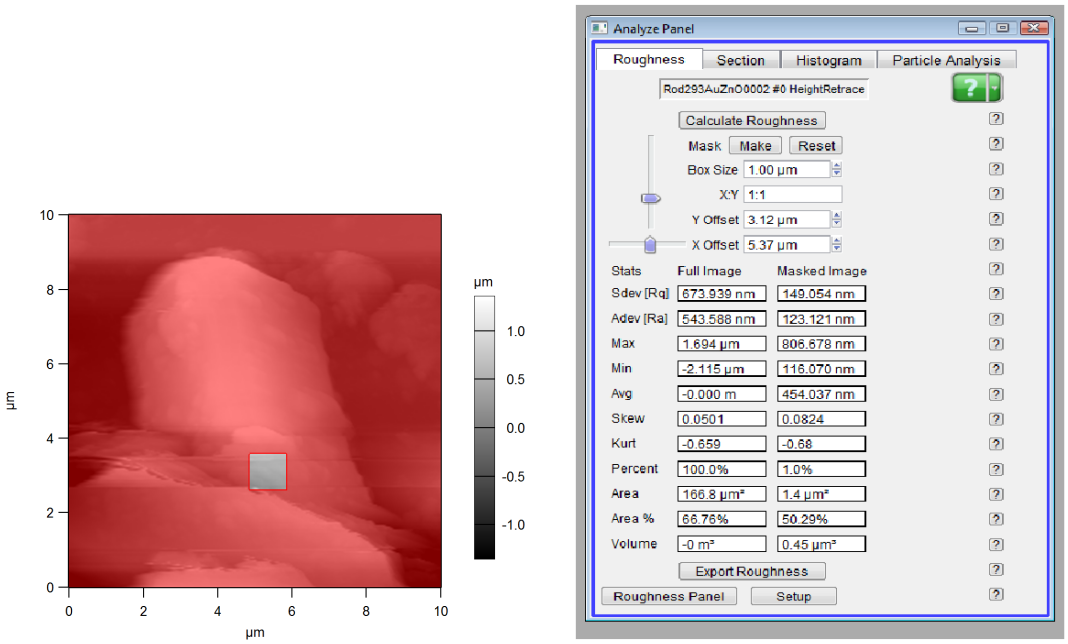

Figure S7: Masking procedure to calculate surface area of Au covered ZnO nanorods. The screen capture is from the Asylum Research procedures within IGOR. In this example, the 1 μm^2 small gray box in the image at left has a surface area of 1.4 μm^2. This approach was used to select data for the work function calculations as well, selecting areas near the centers of crystals.

The roughness factor R_q calculation used the following equation[6],

$$R_q = \sqrt{\frac{1}{n}\sum_{i=1}^{n} Z_i^2} \tag{S3}$$

Here Z is the height deviation from the mean surface (xy plane) of the sample and n is number of points during the scan. Figure S8 shows an example of a height image collected during a KPFM scan. This height data provides the Z values for the above equation. The roughness factors plotted in the main paper (Figure 4) are also presented in Table S1.

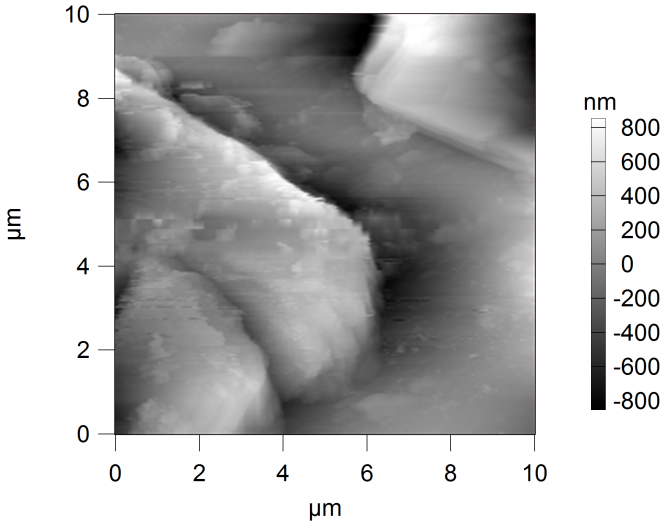

Figure S8: Example of a height image from a KPFM scan of a rod shaped ZnO crystal.

Table S1: Roughness factors of different thicknesses of Au on ZnO.

Sample tag	R_q (nm)
A45	109 ± 9
A35	157 ±16
A25	207 ± 8
A15	138 ±10

References

[1] K. A. Alim, V. A. Fonoberov and A. A. Balandin, *Appl. Phys. Lett.*, 2005, **86**, 053103–1.

[2] A. Souissi, A. Marzouki, A. Sayari, V. Sallet, A. Lusson and M. Oueslati, *J. Raman Spectrosc.*, 2011, **42**, 1574.

[3] J. H. Nobbs, *Rev. Prog. Color. Relat. Top.*, 1985, **15**, 66.

[4] K. A. Willets and R. P. V. Duyne, *Annu. Rev. Phys. Chem.*, 2007, **58**, 267.

[5] E. C. L. Ru, E. Blackie, M. Meyer and P. G. Etchegoin, *J. Phys. Chem. C*, 2007, **111**, 13794.

[6] M. Donoso, A. Méndez-Vilas, J. Bruque and M. González-Martin, *Int. Biodeterior. Biodegrad.*, 2007, **59**, 245.